

Discrimination of pores and cracks in iron ore pellets using deep learning neural networks

<http://dx.doi.org/10.1590/0370-44672019730119>

Emanuella Tarciana Vicente Bezerra^{1,2}

<https://orcid.org/0000-0002-1945-303X>

Karen Soares Augusto^{1,3}

<https://orcid.org/0000-0002-0116-4993>

Sidnei Paciornik^{1,4}

<https://orcid.org/0000-0001-6520-2007>

¹Pontifícia Universidade Católica do Rio de Janeiro – PUC-RJ, Departamento de Engenharia Química e de Materiais, Rio de Janeiro - Rio de Janeiro – Brasil.

E-mails: ²etvb.89@gmail.com,

³saugustokaren@gmail.com, ⁴sidnei@puc-rio.br

Abstract

The discrimination between pores and cracks is an important step in the microstructural analysis of iron ore pellets. While the porosity is fundamental during the reduction process in blast furnaces, cracks are strongly detrimental to the mechanical strength. The usual image processing tools cannot automatically discriminate between these two types of features, especially in 3D images obtained, for instance, with x-ray microtomography (microCT). As pores and cracks have essentially the same x-ray absorbance, they cannot be discriminated by a simple intensity threshold. Given the complex shapes in 3D and the presence of many connections between pores and cracks, shape discrimination is not successful either. Thus, this article proposes the use of Deep Convolutional Neural Networks (DCNN) to discriminate between these 2 classes of discontinuities. The well-known U-NET architecture was employed. The network was trained by manually outlining representative objects of the 2 classes in a few layers of the 3D image. After optimization of the training parameters, the network was applied to the full image, successfully discriminating between pores and cracks. The trained network was then applied to the images of different pellets with good results. However, some residual errors are present. These characteristics are analyzed and possible solutions are proposed.

Keywords: x-ray microtomography, image analysis, deep convolutional networks; porosity; cracks.

1. Introduction

The pelletizing process consists of three main steps: preparation of the raw materials, formation of the green pellet, and heat treatment to harden the pellet. At the end of the process, the pellets are porous and may contain cracks. Pores originate in the preparation of the green pellets, when water fills the voids between the particles. As the burning starts, the water evaporates and is replaced by the air entering the system. (Meyer, 1980) Open pores connected to the surface facilitate the reactions and the heat exchange to which the pellets are submitted in the furnaces, while closed pores do not connect with the surface and exert influence on the macroscopic properties of the pellet. (Klobes *et al.*, 2006) Cracks are discontinuities that influence several characteristics, such as the compressive strength, which affects the pellet integrity during transport and inside the loaded furnace.

Two types of cracks can be found: thermal cracks, resulting from the sudden change of temperature during the heat treatment, which are usually found in the inner part of the pellets; and resilience cracks, formed by the handling and overlapping of the pellets, which cause mechanical ruptures, being generally larger and tending to appear at the surface. (Fonseca, 2019).

The characterization of iron ore pellets allows to evaluate the quality of the pellet from its chemical, physical and microstructural properties. Most of the studies use Optical Microscopy (OM) as the main characterization method. Wagner *et al.* (2008) and Nellros and Thurley (2011) developed semi-automatic methods capable of creating a mosaic, covering the entire cross section of a pellet for analysis and classification of its different phases of composition. Castellanos *et al.* (2018) proposed a correlation between

optical microscopy and scanning electron microscopy techniques to improve the identification of mineral phases and porosity. Iglesias *et al.* (2018) developed an automatic method for microstructural characterization of iron ore. In another study, it was possible to perform a quantitative analysis of the degree of sintering from images obtained. (Nellros *et al.*, 2015) However this technique, besides being destructive, provides only 2D information, limiting the study and the visualization of the internal and complete structure of the pellet. For this reason, x-ray microtomography (microCT) has been used with the advantage of being a non-destructive technique and having the ability to generate three-dimensional images (3D). (Augusto and Paciornik, 2018)

Differentiation between pores and cracks is important for the microstructural analysis of pellets because porosity is a

required feature, while cracks are detrimental to the mechanical properties. Image analysis has been extensively used in this context. The usual sequence involves the following steps (Gomes *et al.*, 2013):

- Pre-processing to reduce image defects, such as uneven background and noise.
- Segmentation, mostly by intensity thresholding, to discriminate the features of interest.
- Post-processing to correct errors from the segmentation step.
- Measurements of size, shape, texture, among others.
- Measurement-based separation of features into classes.

This sequence is successful in many cases but fails under certain conditions. In the case of microCT, pores and cracks have the same x-ray absorbance and share the same intensity range in the images. Thus, they cannot be discriminated by an intensity threshold. In 3D images, measurement-based classification does not work either, given the complexity of the size and shape distributions and, especially, due to the presence of many

interconnections between pores and cracks.

Recently there was a boom in the use of Machine Learning techniques that are able to mimic human recognition tasks. Importantly, once these algorithms are trained, they can learn from experience and make decisions upon new data. (Tacchella *et al.*, 2019) In the domain of image recognition and classification, a great improvement was reached with the so-called Convolutional Neural Networks (CNN). These networks use as input the pixel/voxel intensities/colors and automatically derive higher complexity features that can then be used for classification. (Goodfellow *et al.*, 2016). This approach bypasses the traditional sequence outline above, as it does not require previous segmentation and measurements before classification.

With the evolution of hardware, especially Graphic Processing Units (GPU) that are extremely efficient in parallel processing of data, it has become practical to train deeper networks – meaning networks with several layers between input (that receive pixel/voxel

intensities) and output (that provide the desired object classes). This Deep Learning (DL) architecture is able to process the input pixels/voxels, and, as data propagates through the network layers, build ever more complex features that correspond to the detection of edges, orientations and other high-level descriptors of the objects. (Lecun *et al.*, 2015)

The detailed description of DL networks is out of the scope of this article, but Figure 1 shows a typical architecture. (Cheng *et al.*, 2018) The input image is scanned in sub-windows and its pixel intensities are the input data for the first convolutional layer. This layer is composed of neurons responsible for applying a filter to a specific piece of the image, and this filter derives higher level characteristics of that group of pixels. The convolution results go through a pooling layer that is used to reduce the dimensionality of the data. As data moves to other convolution and pooling layers, more complex features are derived. In the last, fully connected layer, the data is finally processed and attributed to one of the desired classes.

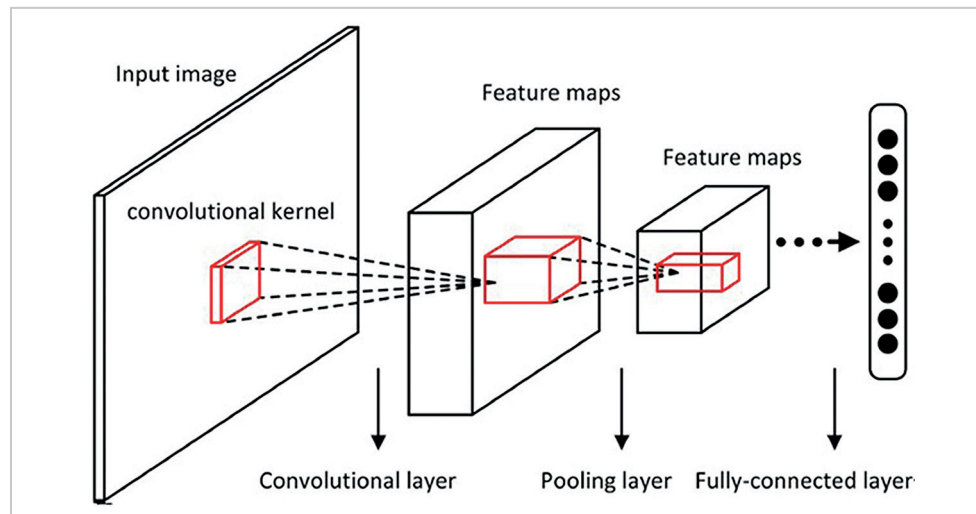


Figure 1 - Structure of a Deep Learning network. (Cheng *et al.*, 2018).

DL networks are supervised classification structures – they require the user to provide examples of objects of each class. As the data moves forward in the network, each connection has an initial random weight that multiplies the value at that point. As the weighed values reach the output, the results are compared to the known trained data and an error is calculated. This is then used to back propagate through the network and adjust the weights so that the error is reduced. This forward and back propagation procedure is repeated for a certain number of

cycles – epochs – until the error reaches a predefined minimum value. (Haykin, 1994; Yegnanarayana, 2009; Goodfellow *et al.*, 2016)

The error minimization and weight adjustment steps are extremely computer intensive as a very large number of parameters must be simultaneously optimized. The deeper the network, the larger the number of parameters. That is where the parallel computation capacity of the GPU's is critical. Given the strong recognition capabilities of DL networks, they have become omnipresent in most

image processing/analysis/classification applications, such as in face recognition, remote sensing, medical image diagnostic, among others. (Sun *et al.*, 2015; Shen *et al.*, 2017; Cheng *et al.*, 2018)

Therefore, herein, we show the application of DL networks to the discrimination between pores and cracks in iron ore pellets imaged by microCT. A specific DL architecture was selected, the network was trained with limited user defined examples, the training parameters were optimized, and the network was applied to other images.

2. Materials and methods

2.1 Samples and microCT image acquisition

The pellets analyzed in the present study were provided by Vale. A Zeiss XRadia 510 Versa microtomograph was used to acquire the 3D images. The x-ray source was set to 150 kV, 10 W. Using the so-called macro lens of the equipment (0.4X), it was possible to image full pellets with ~1 cm diameter. With 360° rotation, 4000 projections and binning 1 for acquisition and reconstruction,

a pixel size of 7 μm was reached, corresponding to approximately 14 μm spatial resolution. The acquisition conditions were the same for all pellets: total scan time of 10.6 h followed by the reconstruction procedure, that took a few minutes. The scan time can be optimized by changing the number of projections and other parameters, but we found that the parameters used were a good

compromise between time, spatial resolution and signal to noise ratio. Each 3D image contained 2008 slices with 2048 by 2004 pixels and 16 bits. (Augusto and Paciornik, 2018). Except for gluing to a support, no further specimen preparation was necessary.

The images were separated into 2 groups: training and test, as described in the following.

2.2 Digital image processing and Deep Learning

Image processing and DL network development was carried out in Dragonfly 4.0 (Object Research Systems, Montreal). To prepare the images for DL training and application, a few image processing steps were necessary.

Using traditional intensity thresholding and logic operations, both the solid part of the pellet and the pores/cracks were segmented and treated as Regions of Interest

(ROI's). The procedure is depicted in Figure 2. Figure 2a shows the segmented solid. The dark pores and cracks cannot be directly segmented because pixels external to the pellet share the same intensity range. Thus, first, inner voids were filled (Figure 2b). At this point pores and cracks connected to the pellet surface are not correctly detected. Then a morphological operation that closes open voids within a certain size range was used,

leading to the image shown in Figure 2c. Finally, a logical subtraction was performed between the images corresponding to the solid and the filled solid. Thus, a new ROI was formed (Figure 2d) containing the voids, pores and cracks, present in the pellet. The mask from Figure 2c was also used to bring to zero the pixels outside of the pellet, thus avoiding any confusion with the intensities of pores or cracks.

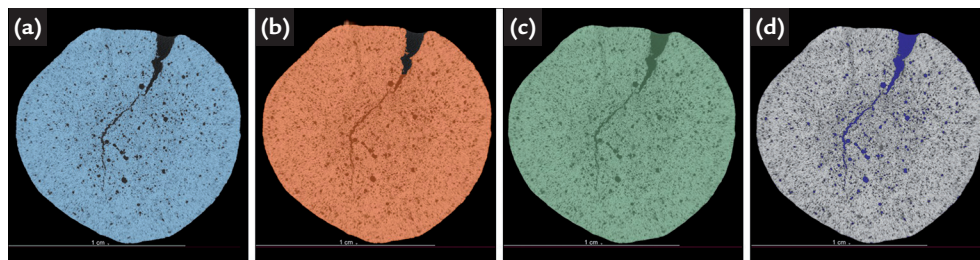


Figure 2 - Segmented images: a) segmented solid; b) internal voids filled; c) connected voids filled; d) pores and cracks, in blue, obtained subtracting a from c.

As the objective of the training is to provide sufficient data to the model for automatic discrimination of pores and cracks, these ROIs were used as input data for the training and for this, 5 random layers were chosen within the layer set image, and part

of the pores and cracks contained in the layers were segmented (Figure 3). The pores and cracks were obtained separately using a manual segmentation within the mask created in Figure 2c. The software has tools for this manual segmentation, which are

found in the ROI painter function. The tool used acts as a brush, which can be adjusted within the desired region to be segmented. Thus, some pores and cracks were segmented (painted) in each of the 5 layers chosen, diversifying according to their shape and size.

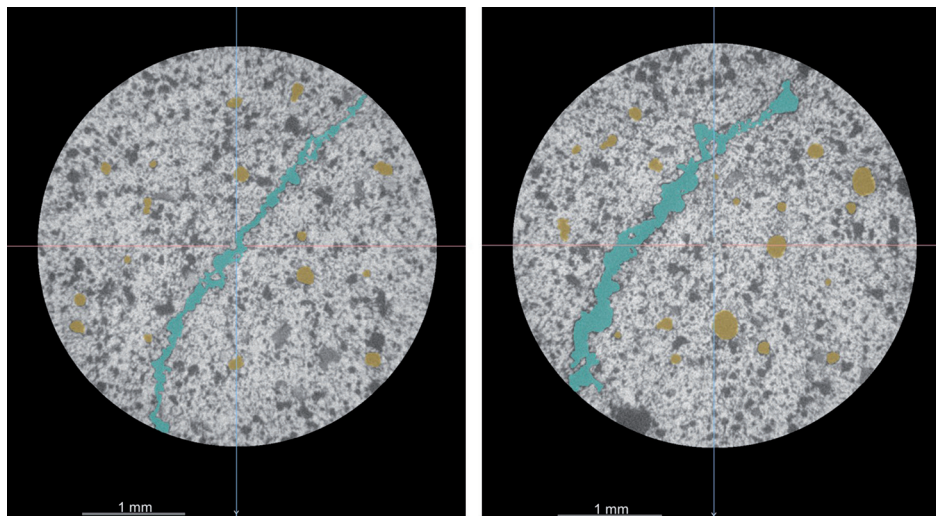


Figure 3 - Examples of layers chosen for segmentation containing parts of the segmented pores and cracks: blue corresponds to cracks and yellow to pores.

This input data was then provided to the network. The architecture used was based on the U-Net, defined by Ronneberger (2015), which is well-known for producing good results with limited amount of data. The U-Net (Figure 4) is comprised of 2 branches:

contraction or down-sampling, which consists of a typical convolutional network architecture, containing convolution layers and max pooling, gradually reducing the image size with increasing depth; and expansion or up-sampling, where transposed and

regular convolutions are applied, so as to gradually increase the image size and decrease the depth. Besides, for more precise location of detected features, concatenation layers are used, which allow direct connections between the two branches.

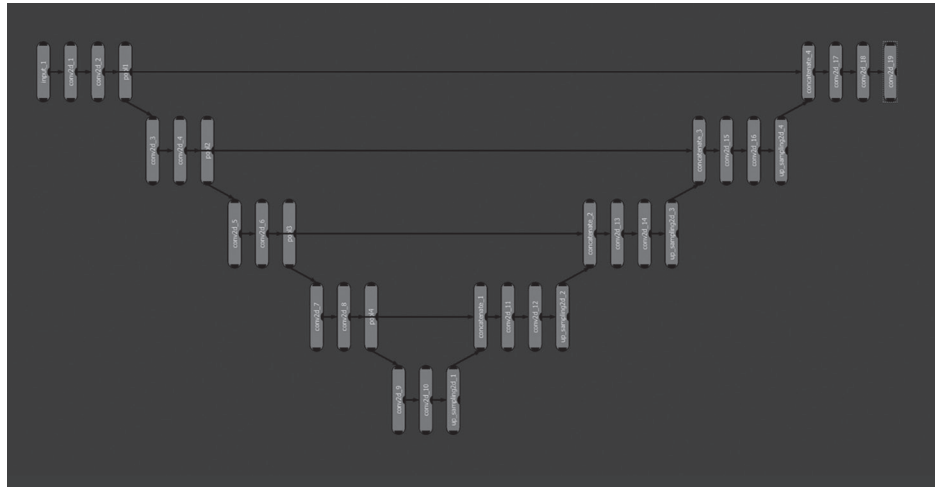


Figure 4 - U-Net architecture of the DL model used.

The first model was based on the data described above and a preliminary result was obtained, in which discrimination between pores and cracks was already evidenced (Figure 5). However, many defects were found such as misclassification

of pores and cracks or incomplete segmentation of certain features. Then, starting from this preliminary result, 15 layers were chosen, containing some of the most relevant errors and their variations, and these errors were corrected

by manual segmentation, as described above. Figure 5 shows one of the chosen layers: the first presents the segmentation containing some highlighted faults in the green circles and the second, the corrected segmentation.

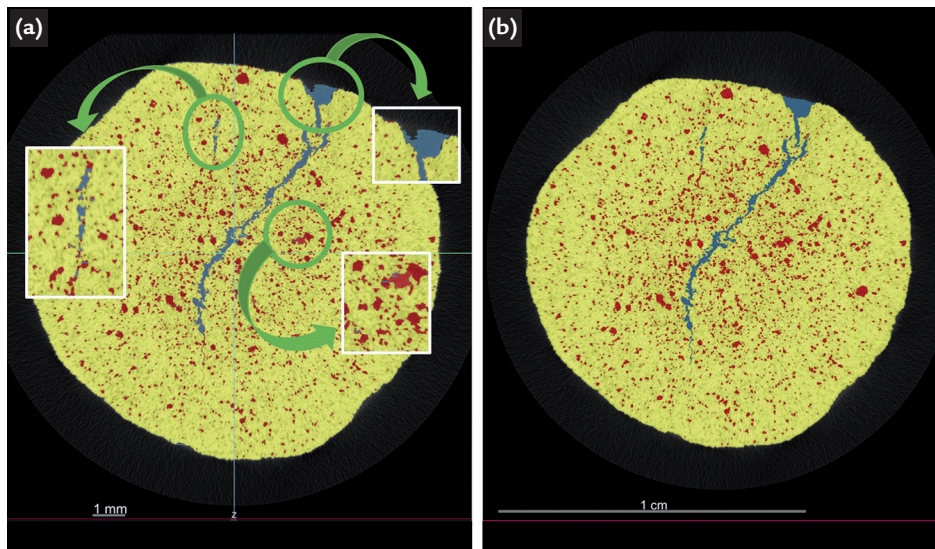


Figure 5 - Preliminary result from the first model created: blue corresponds to cracks and red to pores in both images: a) Segmentation containing errors in segmentation. b) Manually corrected segmentation.

The corrected layers were then fed to the U-Net and training parameters were selected. Again, the details are out of the scope of the article, but the main numbers are shown in Table 1. The input size corresponds to the size of the analysis window that is scanned upon the image. It must be large enough to contain representative features to

be detected but not too large as this increases the computational complexity. The stride to input ratio represents the scanning step, 1 representing a step as large as the input size and smaller values meaning overlap between scanning steps. The number of epochs is the number of forward and backward iterations for weight adjustment and error

minimization. It must be large enough to allow for error minimization, but not too large to avoid the phenomenon of overfitting, in which a network mode is optimized down to a very small error, losing its generalization capacity. Overfitted networks are very efficient for the same image used for training but fail for different test images.

Table 1 - DL network training parameters

Parameters	Value
Input size	256
Stride to input ratio	1
Number of Epochs	50

3. Results and discussion

Figure 6 shows the results of the application of the optimized network to

3 different layers of the reference pellet, from which the training layers were se-

lected. Figure 7 depicts 3D renderings of this pellet showing pores and/or cracks.

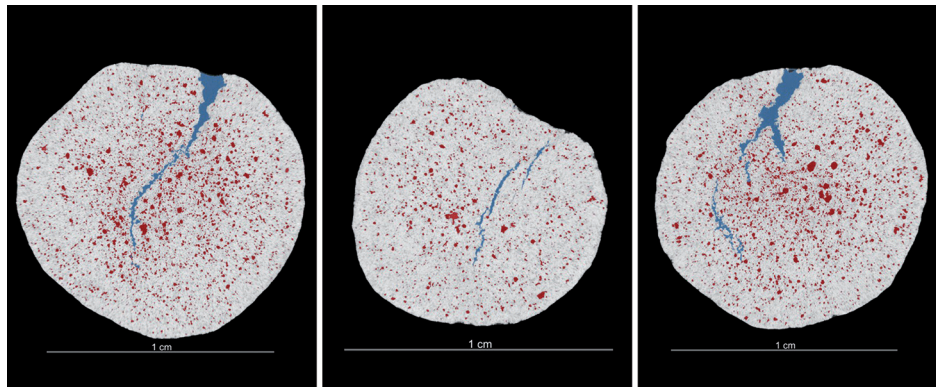


Figure 6 - Application of trained DL network to 3 different layers of the reference sample where red is pores, blue is cracks and grey corresponds to solid.

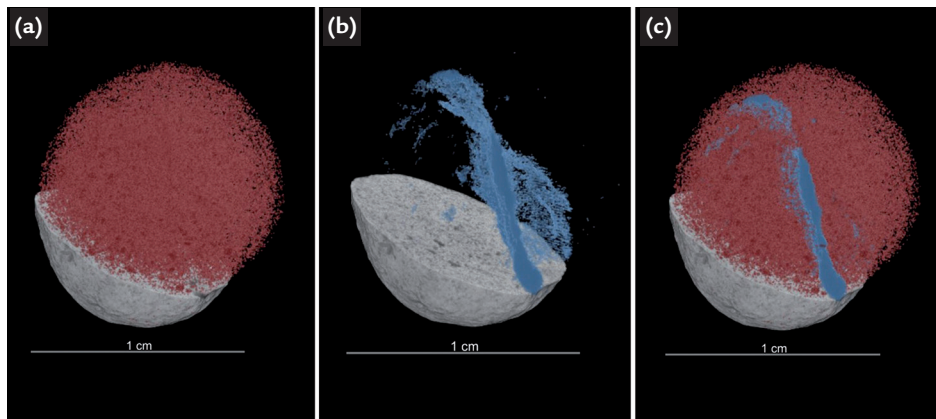


Figure 7 - 3D renderings. a) Pores (red); b) Cracks (blue); c) Both.

Training is the most time-consuming step in the application of DL. The manual preparation of training data is a lengthy and tedious operation. The training of the network can also take substantial time depending on the image size and hardware capabilities. This training of the network lasted around 50 minutes, using a dual Intel® Xeon® CPU E5-2660 v3 @ 2.60GHz and 4 NVIDIA GeForce GTX 980 Ti GPU's. However, once the network is trained, in principle it can be directly and efficiently applied to similar images of other pellets. This generalization capability

is, indeed, one of the main advantages of the neural network approach.

Thus, the DL model trained as described above was also applied to 4 other pellets tomographed under the same conditions. The results are shown in Figure 8 and are very promising. Pores and cracks were successfully discriminated, whereby even small pores and thin cracks were detected. In some cases, however, such as in Figure 8c, thicker parts of the cracks were not accurately detected.

There are several possible explanations for these errors. First, as the whole

DL approach is based on pixel intensities, brightness/contrast variations between the training reference pellet and the tested ones would affect the result. Second, it is hard to establish how much training data is enough. Evidently, the less the better, as this minimizes the labor-intensive step of manual segmentation, but a limited training dataset will miss some important features, especially for objects with complex shapes. Third, as briefly mentioned above, the network training involves many parameters that must also be optimized, and the strategy is not always well defined.

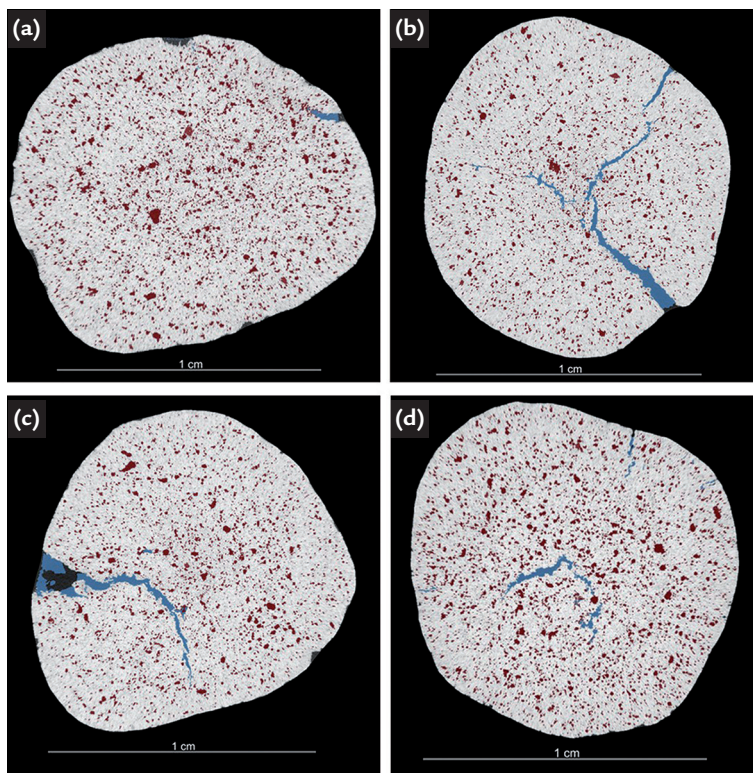


Figure 8 - Application of the trained DL model to other pellets. a) P2; b) P3; c) P4; d) P5.

4. Conclusions

We have shown that Deep Learning neural networks can be successfully applied to the discrimination between cracks and pores in microCT images of iron ore pellets. The methodology can be easily adapted to other kinds of materials in which pores and cracks are relevant, such as in cementitious materials, rocks and sintered metals or ceramics.

Even though the training step is tedious and lengthy, the results show that it does not need to be repeated once a reasonable amount of training data has been provided to the network. A possible improvement in the results for other pellets may involve other strategies, such as including in the training data a few manually annotated layers

from a different pellet. A technique called histogram specification (Hildebolt *et al.*, 1996) can also be applied to guarantee that the intensity histograms of the reference training sample and those of the test samples are very similar. Thus, the errors associated to brightness/contrast variations will likely be reduced.

Acknowledgments

The support of Brazilian funding agencies CNPq, CAPES and FAPERJ is gratefully acknowledged. The authors are

especially indebted to Benjamin Provencher, Normand Mongeau, Nicolas Piche and Mike Marsh, from Object Research

Systems (Montreal) for the support with the Deep Learning model development and training in Dragonfly software.

References

- AUGUSTO, K. S.; PACIORNIK, S. Porosity characterization of iron ore pellets by x-ray microtomography. *Materials Research*, São Carlos, v. 21, n. 2, p. 1-9, jan. 2018.
- CASTELLANOS, R. M.; INGLESIAS, J. C. A.; GOMES, O. F. M.; AUGUSTO, K. S.; PACIORNIK, S. Characterization of iron ore pellets by multimodal microscopy and image analysis. *REM - International Engineering Journal*, v. 71, p. 209-215, 2018.
- CHENG, G.; YANG, C.; YAO, X.; GUO, L.; HAN, J. When deep learning meets metric learning: remote sensing image scene classification via learning discriminative CNNs. *IEEE Transactions on Geoscience and Remote Sensing*, v. 56, n. 5, p. 2811-2821, jan. 2018.
- FONSECA, M. C.; COSTA, G. M.; FERREIRA, P.; MESCHIATTI, A. The influence of pellet feed size distribution in the agglomeration process. In: IRON & STEEL TECHNOLOGY CONFERENCE - AISTECH, 2005, Charlotte, USA. *Proceedings[...]*. Warrendale, PA: Association for Iron & Steel Technology, 2005. v. 1, p. 147-153.
- GOODFELLOW, I.; BENGIO, Y.; COURVILLE, A. *Deep learning*. Cambridge: MIT Press, 2016.
- GOMES, O. D. M.; IGLESIAS, J. C. A.; PACIORNIK, S.; VIEIRA, M. B. Classification of hematite types in iron ores through circularly polarized light microscopy and image analysis. *Minerals Engineer*, v. 52, p. 191-197, sep. 2013.
- HAYKIN, S. *Neural networks: a comprehensive foundation*. New York: MacMillan, 1994.

- HILDEBOLT, C. F.; WALKUP, R. K.; CONOVER, G. L.; YOKOYAMA-CROTHERS, N.; BARTLETT, T. Q.; VANNIER, M. W.; SHROUT, M. K.; CAMP, J. J. Histogram-matching and histogram-flattening contrast correction methods: a comparison. *Dentomaxillofacial Radiology*, v. 25, n. 1, p. 42-47, 1996.
- INGLESIAS, J. C. A.; AUGUSTO, K. S.; GOMES, O. F. M.; DOMINGUES, A. L. A.; VIEIRA, M. B.; CASAGRANDE, C.; PACIORNIK, S. Automatic characterization of iron ore by digital microscopy and image analysis. *Journal of Materials Research and Technology*, v. 7, p. 376-380, 2018.
- KLOBES, P.; MEYER, K.; MUNRO, R. G. *Porosity and specific surface area measurements for solid materials*. Washington: National Institute of Standards and Technology, 2006.
- LECUN, Y.; BENGIO, Y.; HILTON, G. Deep learning. *Nature: International Journal of Science*, v. 521, p. 436-444, may 2015.
- MEYER, K. *Pelletizing of iron ores*. New York: Springer – Verlag Berlin Heidelberg, 1980.
- NELLROS, F.; THURLEY, M. J. Automated image analysis of iron-ore pellet structure using optical microscopy. *Minerals Engineering*, v. 24, p. 1525-1531, 2011.
- NELLROS, F.; THURLEY, M. J.; JONSSON, H.; ANDERSON, C.; FORSMO, S. P. E. Automated measurement of sintering degree in optical microscopy through image analysis of particle joins. *Pattern Recognition*, v. 48, p. 3451-3465, 2015.
- RONNEBERGER, O.; FISCHER, P.; BROX, T. U-Net: convolutional networks for biomedical image segmentation. In: NAVAB N.; HORNEGGER J.; WELLS W.; FRANGI A. (ed.) *Medical Image Computing and Computer-Assisted Intervention – MICCAI 2015*. Springer, Cham, 2015. v. 9351, p. 234-241. (Lecture Notes in Computer Science).
- SHEN, D.; WU, G.; SUK, H. Deep learning in medical image analysis. *Annual Review of Biomedical Engineering*, v. 19, p. 221-248, mar. 2017.
- SUN, Y.; LIANG, D.; WANG, X.; TANG, X. DeepID3: face recognition with very deep neural networks. *ArXiv*, v. abs/1502.00873, 2015.
- TACCHELLA, A.; ROMANO, S.; FERRALDESCHI, M.; SALVETTI, M. Collaboration between a human group and artificial intelligence can improve prediction of multiple sclerosis course: a proof-of-principle study. *F1000Research*, v. 6, p. 2172-2185, may. 2019.
- WAGNER, D. T.; ROUCO, H. V.; GOMES, O. F. M.; PACIORNIK, S.; VIEIRA, M. B. Caracterização de pelotas de minério de ferro por microscopia digital e análise de imagens. *Tecnologia em Metalurgia e Materiais*, v. 5, p. 215-218, 2008.
- YEGNANARAYANA, B. *Artificial neural networks*. New Delhi: Prentice-Hall of India, 2009. 476 p.

Received: 23 August 2019 - Accepted: 18 November 2019.